

# Enhancement of Rheological and Mechanical Properties of Bitumen by Polythiophene Doped with Nano Fe<sub>3</sub>O<sub>4</sub>

SEYYED MOJTABA MOUSAVI,<sup>1</sup> SEYYED ALIREZA HASHEMI,<sup>1</sup>  
AZIZ BABAPOOR,<sup>1</sup> and BIJAN MEDI<sup>2,3</sup>

1.—Department of Chemical Engineering, University of Mohaghegh Ardabili, P.O. Box 179, Ardabil, Iran. 2.—Department of Chemical Engineering, Hamedan University of Technology, P.O. Box 65155-579, Hamedan, Iran. 3.—e-mail: medi@hut.ac.ir

Bitumen has remarkable chemical and mechanical properties as a construction and insulating material. In this research, bitumen reinforced with polythiophene, which is doped with Fe<sub>3</sub>O<sub>4</sub> nanoparticles, was produced by the vacuum shock technique. Samples were prepared at various filler loadings to investigate their rheological and mechanical properties. Characteristics of the samples were evaluated using a dynamic shear rheometer and various empirical rheological tests including the softening point, penetration, and reversibility. The results indicated that the synthesized nanoparticles have good compatibility and interaction with the molten phase of bitumen. On the other hand, modification of bitumen has led to significant improvement in the compound shear modulus and resistance against deformation, while it has hindered fatigue damage and improved the softening point, penetration, and reversibility.

## INTRODUCTION

Bitumen is a viscous, adhesive, and heterogeneous mixture of hydrocarbons, which consists of condensed aromatic, aliphatic, and naphthenic compounds.<sup>1</sup> Bitumen is used for various purposes including coating, road construction, and waterproofing applications.<sup>1,2</sup> It is used as a binder for the abovementioned applications because of its thermo-plastic and reversible properties.<sup>3,4</sup> It controls the final properties of asphalt since bitumen is a deformable material and produces a continuous matrix in asphalt.<sup>5</sup>

The overall mechanical properties and microstructure of bituminous materials are highly dependent on their compositions.<sup>6</sup> The chemical constituents of bitumen can be classified into two groups: maltenes and asphaltenes. Maltenes can be further divided into resins, aromatics, and saturates.<sup>1,2,7,8</sup> Resins are polar and highly adhesive, while asphaltenes are highly polar. Any increase in the asphaltene ratio can increase the hardness, softening point, and final viscosity of binders. Moreover, asphaltenes can also decrease the penetration rate of bituminous materials. On the other hand, aromatics can exist in bitumen as either polar

or non-polar compounds, while the polar aromatics are comparatively more viscous. Aromatics and saturates are considered the plasticizers of bituminous suspensions. Saturates are mostly straight, non-polar, and branched-chain aliphatic hydrocarbons, which include most of the bitumen waxy fraction.<sup>1,2,7</sup> The concentration and arrangement of bitumen compounds in the oily phase along with the environmental condition affect the rheological properties of bituminous materials in a wide range.<sup>8</sup>

Bituminous binders suffer from diverse kinds of failures including rutting, thermal cracking, and fatigue damage, which decrease the average lifespan of asphalts and reduce the quality of pavements.<sup>1,2,9,10</sup> Therefore, various kinds of minerals and polymeric additives are added to bitumen to improve its overall mechanical and thermal properties and hence enhance its average lifespan.<sup>1,4,8,11–21</sup> Similarly, aging can also affect the overall properties of bituminous binders in particular because of UV-Vis degradation, which is prevented by light-resistant materials.<sup>22–25</sup>

Mousavi et al.<sup>21</sup> modified the 70 penetration-grade bitumen with styrene acrylonitrile copolymer. Their results revealed that the modified bitumen showed significant improvement in terms of

stability and flexibility at high and low temperatures, respectively, while the phase angle decreased from  $55^\circ$  to  $35^\circ$  for the modified samples compared with the unmodified samples. Furthermore, in several studies, reinforced bitumen with clay nanoparticles<sup>1,11,16</sup> presented better stiffness, aging resistance, complex shear modulus, and elasticity compared with the neat bitumen, while the phase angle also decreased.

Zhu et al.<sup>18</sup> investigated the effect of zinc oxide nanoparticles along with organic expanded vermiculite on the rheological properties of various kinds of bituminous materials including 70, 90, and 110 penetration grades. Their results suggested that rutting resistance was enhanced because of the addition of anti-aging fillers. Additionally, due to the application of these additives, the complex shear modulus and phase angle decreased and increased, respectively.

Polythiophene (PT), which is one of the most important heterocyclic polymers with heteroatoms in the polymer main chain, has remarkable extended  $\pi$  conjugation.<sup>26–29</sup> Moreover, PT presents outstanding flexibility, thermal stability, optical properties, and electrical conductivity represented by a high Seebeck coefficient compared with other conductive polymers.<sup>30–36</sup>

PT can be decorated with coumarin, naphthalene, and pyrene. Pyrene is a fluorescent compound with four fused aromatic rings. Its presence along with moieties and naphthalene not only improves the interaction and compatibility between PT and bitumen, but also increases the overall absorption rate in the UV–Vis region. It can also improve the charge transfer process and stacking interaction, thus decelerating the aging process of bitumen compounds.<sup>37–39</sup>

PT as a perfect electromagnetic wave shield can meet the aforementioned requirement, but it suffers from dielectric loss. In this case, to enhance the absorption properties of PT, it is essential to modify PT with magnetic materials such as  $\text{Fe}_3\text{O}_4$  to reduce its magnetic loss.<sup>5</sup>

Addition of polythiophene- $\text{Fe}_3\text{O}_4$  (PT-F) to bitumen at different weight percentages can improve the interaction between the molten phase and distributed particles and decelerate the aging process of bitumen because of its strong absorption rate in the UV–Vis region. Similarly, the presence of naphthalene along with its functional groups can improve the compatibility and interaction of PT-F with bitumen.<sup>37–39</sup>

In this study, we first describe the process of doping polythiophene with  $\text{Fe}_3\text{O}_4$ , but the main objective is modifying 70 penetration-grade bitumen. In this regard, the overall performance of the samples was evaluated using a dynamic shear rheometer (DSR) and diverse empirical rheological tests. Specification and morphology of PT-F were examined via several techniques, and their effects on the properties of bitumen including the complex

shear modulus, phase angle, dissipated energy, softening point, penetration, and reversibility were also investigated.

## MATERIALS AND METHODS

### Synthesis Procedures

Synthesis of PT-F was performed via a multi-stage manufacturing method; first, 1 g sodium dodecyl sulfate was ultrasonicated in 100 mL ethanol solution at 200 W for 10 min at  $45^\circ\text{C}$ , while 42 mL hexadecane and 5.6 mL thiophene monomer were mixed with each other and then ultrasonicated at 200 W for 10 min at the same temperature. Then, both suspensions were poured in a beaker containing 320 mL deionized water and ultrasonicated at 400 W for 20 min at  $60^\circ\text{C}$ . Then, 3.89 g  $\text{FeCl}_3$  (4  $\text{H}_2\text{O}$ ) and 4.55 g  $\text{FeSO}_4$  (6  $\text{H}_2\text{O}$ ) were poured in the resulting suspension and stirred for 1 h at 500 rpm and  $80^\circ\text{C}$ . In the next step, 50 mL  $\text{NH}_3$  was added to the final suspension and stirred for 48 h at 500 rpm and  $80^\circ\text{C}$ . The final suspension was vacuum filtered and simultaneously washed with deionized water to set the pH of the synthesized PT-F at 7.

Moreover, to compare the FTIR results of  $\text{Fe}_3\text{O}_4$  with PT-F,  $\text{Fe}_3\text{O}_4$  nanoparticles were synthesized via a simple method; 3.89 g  $\text{FeCl}_3$  and 4.55 g  $\text{FeSO}_4$  were poured in 320 mL deionized water and stirred for 1 h at  $80^\circ\text{C}$ . Then, 40 mL  $\text{NH}_3$  was added to the resulting suspension and stirred for 24 h at  $80^\circ\text{C}$ . Subsequently, the suspension was vacuum filtered and washed with deionized water to set the final pH of the synthesized  $\text{Fe}_3\text{O}_4$  at 7. An overview of PT-F and  $\text{Fe}_3\text{O}_4$  synthesis procedures is shown in Figs. S1 and S2 of the Supplementary material, respectively.

For modifying bitumen with PT-F nanoparticles, first PT-F (at 3 wt.%, 5 wt.%, 7 wt.%, and 10 wt.%) was poured in 100 mL acetone and ultrasonicated at 200 W (with  $45^\circ\text{C}$  temperature limit) for 10 min. Then, the neat bitumen was heated up to  $160^\circ\text{C}$ , and PT-F/acetone suspension was added to it at several ratios. In the next step, the prepared suspension was placed in a sealed chamber with a mixing shaft inside. It was first dispersed for 30 min at 500 rpm and then dispersed for 60 min at 4000 rpm with 20–60 cmHg vacuum shock to obtain a homogeneous and voidless composition. Application of the vacuum shock technique reduces the overall amount of bubbles and voids and wipes out the stress concentration areas. In the vacuum shock technique, rapidly rising and falling negative pressures were used to improve the mobility of bubbles throughout the suspension and decrease voids within the composite structure. In this case, the vacuum level was varied between 20 cmHg and 60 cmHg. More details about this method can be found in our previous works.<sup>40–43</sup> Afterwards, the resulting suspension was poured in steel casts with 1-mm and 2-mm spacings and then heated up and pressed to obtain sheets with uniform thickness. Finally, bitumen sheets holding PT-F at various

filler loadings were solidified at 10°C. The sample synthesis procedure is illustrated in Fig. 1.

### Materials

In this study, the traditional 70 penetration-grade bitumen was supplied by Iranian Bandar Abbas Refinery; its physical properties are given in Table I. All other compounds for synthesis of PT-F and Fe<sub>3</sub>O<sub>4</sub> were supplied by Merck.

### Analysis and Characterization

The viscoelastic behavior of samples containing neat and modified bitumen was evaluated using a dynamic shear rheometer (DSR) based on the ASTM D7175 standard. The DSR test can be used to examine both viscous and elastic performance of bitumen via measurement of the complex shear modulus ( $G^*$ ) and phase angle ( $\delta$ ) at given temperature, stress, strain, and loading frequency ranges. The applied load can be either sinusoidal (oscillatory) or creep and recovery mode. Sinusoidal load is commonly applied under strain-controlled loading mode, while the creep and recovery mode is applied under stress-controlled loading mode.<sup>23,44,45</sup> From the DSR test, torque ( $T$ ) and angular rotation ( $\theta$ ) are obtained, which can be used for the calculation of other parameters (e.g., stress and strain). The stress and strain can be calculated based on the recorded torque and angular rotation via the following formulas:<sup>44</sup>

$$\sigma = \frac{2T}{\pi r^3}, \quad (1)$$

$$\gamma = \frac{\theta r}{h}, \quad (2)$$

where  $\sigma$ ,  $T$ ,  $r$ ,  $\gamma$ ,  $\theta$ , and  $h$  are the maximum shear stress (N/mm<sup>2</sup>), torque (N/m<sup>-1</sup>), radius of the parallel plates (mm), shear strain (N/mm<sup>2</sup>), deflection

angle (radians), and gap between parallel plates (mm). Equations 1 and 2 show that the overall values of shear stress and strain highly depend on the geometry of the oscillating plates, which can be chosen based on the stiffness of materials.<sup>46</sup> In this research, 8-mm parallel plates with a 2-mm gap in between were used in the temperature range of 0–40°C in accordance to the stiffness of the neat bitumen and modified samples, which is between 0.1 MPa and 30 MPa.

On the other hand, various viscoelastic parameters can be calculated via the DSR analysis including the complex shear modulus ( $G^*$ ), storage modulus ( $G'$ ), loss modulus ( $G''$ ), phase angle ( $\delta$ ), and dissipated energy.  $G^*$  is defined as the calculated ratio via dividing the absolute value of peak-to-peak shear stress by the absolute value of the peak-to-peak shear strain. It is an indication of stiffness or resistance against deformation under applied load<sup>8</sup> whose absolute value can be calculated via the following equation:<sup>44</sup>

$$G^* = \frac{\sigma_{\max}}{\gamma_{\max}}. \quad (3)$$

Moreover, the storage modulus ( $G'$ ) is the indicator of elastically stored and released energy, which can be referred to as the elastic component of the complex shear modulus. The loss modulus ( $G''$ ) is known as the out-of-phase component of the imaginary part or viscous modulus of the complex shear modulus.<sup>47</sup> Relations between these two parameters and complex shear modulus can be described as follows:<sup>44</sup>

$$G' = |G^*| \cos \delta, \quad (4)$$

$$G'' = |G^*| \sin \delta, \quad (5)$$

$$|G^*| = \sqrt{(G')^2 + (G'')^2}, \quad (6)$$

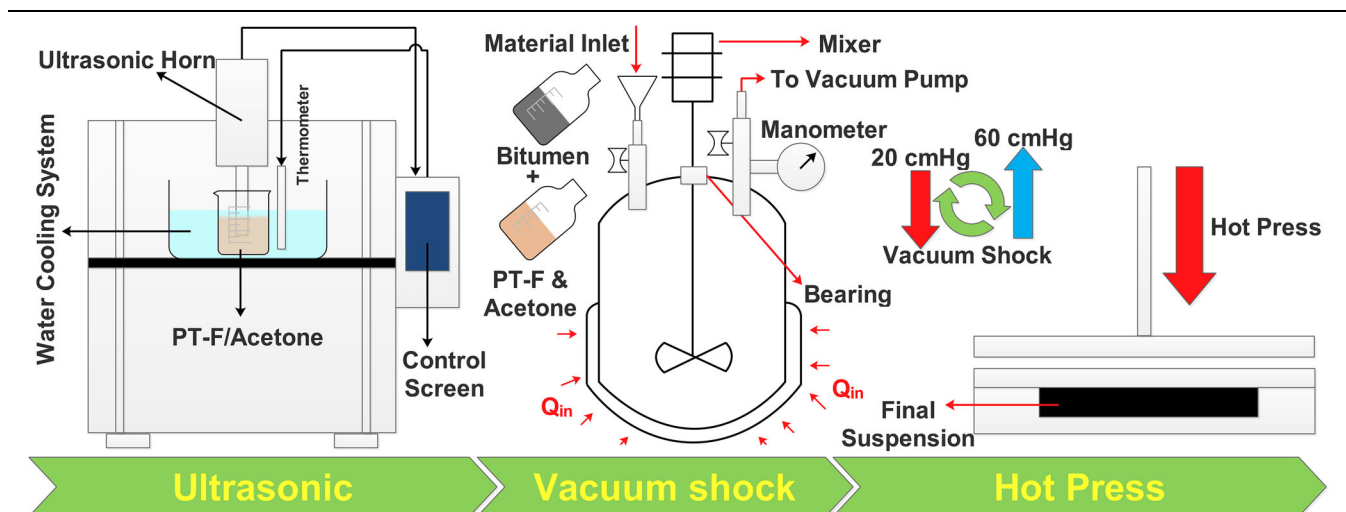


Fig. 1. Production procedure of reinforced bitumen with PT-F at different filler loadings.

**Table I. Physical properties of 70 penetration-grade bitumen**

Type of property	Standard	Unit	Value
Specific gravity (at 25°C)	ASTM D70	g/cm <sup>3</sup>	1.023
Penetration (at 25°C)	ASTM D5	°C	70
Ductility (at 25°C)	ASTM D113	cm	100
Softening point	ASTM D36	°C	49
Kinematic viscosity (at 120°C)	ASTM D2170	mm <sup>2</sup> /s	814
Kinematic viscosity (at 135°C)	ASTM D2170	mm <sup>2</sup> /s	441
Kinematic viscosity (at 160°C)	ASTM D2170	mm <sup>2</sup> /s	218
Performance grade (PG)	ASTM D6373	°C	22–58

where  $\delta$  is the phase angle. The phase angle is in fact the phase lag between sinusoidal strain and stress, which is an indicator of viscoelastic characteristics.

The dissipated energy is an ideal test for examination of fatigue damage. It can be used to evaluate the bituminous materials regardless of the loading mode, temperature, frequency, and rest periods.<sup>48–50</sup> When cyclic loading applies to the viscoelastic materials, they generate diverse pathways for loading and unloading cycles, which can lead to hysteresis loops.<sup>51</sup> Dissipated energy per cycle is measured as the area within the hysteresis loop and can be defined via the following equation:

$$w_i = \pi \sigma_i \varepsilon_i \sin \delta_i, \quad (7)$$

where  $w_i$ ,  $\sigma_i$ ,  $\varepsilon_i$ , and  $\delta_i$  are the dissipated energy, stress amplitude, strain amplitude, and phase angle at cycle  $i$ , respectively. Moreover, the fatigue analysis was performed based on the four-point bending test according to the standard EN 12697-24, in which loading conditions were based on a sinusoidal waveform at 20°C and 10 Hz with stress (1–1.5 MPa) and strain (200–500  $\mu\text{m}/\text{m}$ ) controlled tests.

The temperature sweep test was performed at 10 rad/s with temperature increments of 2°C from 0°C to 45°C. The frequency sweep test was performed at 0.1 rad/s from 1 Hz to 30 Hz while the temperature was set at 20°C. In addition sinusoidal cycles of 10 rad/s were applied to samples in strain control mode to evaluate their resistance until failure. Additionally, empirical rheological tests were performed to measure the softening point and penetration of developed samples based on ASTM D36 and ASTM D5 standards, respectively.

Characteristics of the fabricated PT-F nanoparticles were evaluated using Fourier-transform infrared spectroscopy (FTIR, Bruker model VECTOR22) and a scanning electron microscope (SEM, HITACHI model S-4160). For further evaluation of samples morphology, a 1000 $\times$  digital optical microscope (Rhos, model U1000X) was used. A particle size analyzer (PSA) (Horiba model LB550) based on dynamic light scattering (DLS) was also

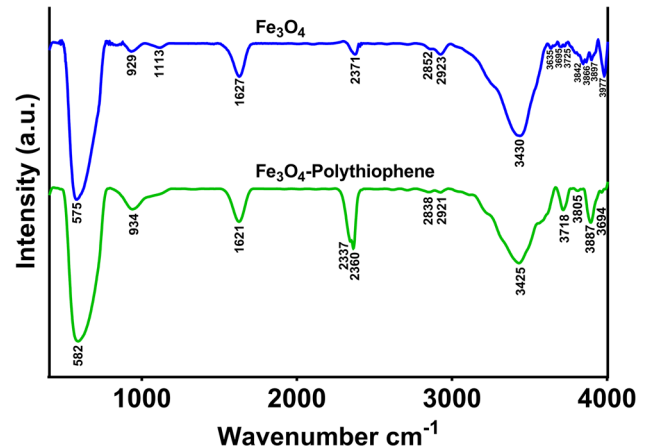


Fig. 2. FTIR results of the synthesized PT-F and Fe<sub>3</sub>O<sub>4</sub> nanoparticles.

used to determine the average size of synthesized PT-F nanoparticles.

## RESULTS AND DISCUSSION

### Sample Characterization

Figure 2 shows the FTIR results of Fe<sub>3</sub>O<sub>4</sub> and PT-F. The strong and broad absorption peak in the region between 3200 cm<sup>-1</sup> and 3550 cm<sup>-1</sup> belongs to the O–H (hydroxyl) stretching intermolecular bond.<sup>33,39,52–55</sup> In this regard, this peak for PT-F has shifted to 3425 cm<sup>-1</sup>, while for Fe<sub>3</sub>O<sub>4</sub> this peak is at 3430 cm<sup>-1</sup>. Weak peaks in the region between 3500 cm<sup>-1</sup> and 3700 cm<sup>-1</sup> belong to the amine N–H stretches. Moreover, the peaks in the region between  $\sim$  2838 cm<sup>-1</sup> and 2921 cm<sup>-1</sup> belong to the C–H stretching vibration (*sp*<sup>3</sup> stretching of hexyl aliphatic side). In the Fe<sub>3</sub>O<sub>4</sub> spectrum, the peak with wavenumber 1627 cm<sup>-1</sup> belongs to the Fe–O,<sup>52</sup> while in the PT-F spectrum the peak at wavenumber 1621 cm<sup>-1</sup> belongs to the C=C stretching.<sup>53</sup> On the other hand, two absorption band peaks at 1113 cm<sup>-1</sup> and 929 cm<sup>-1</sup> in the Fe<sub>3</sub>O<sub>4</sub> spectrum are related to the stretching vibration of the in-plane C–H and *sp*<sup>2</sup> alkene C–H band (disubstituted-E), respectively. Moreover, peaks in the region between 530 cm<sup>-1</sup> and 630 cm<sup>-1</sup> correspond to the stretching vibration mode of Fe–O. In this case, the



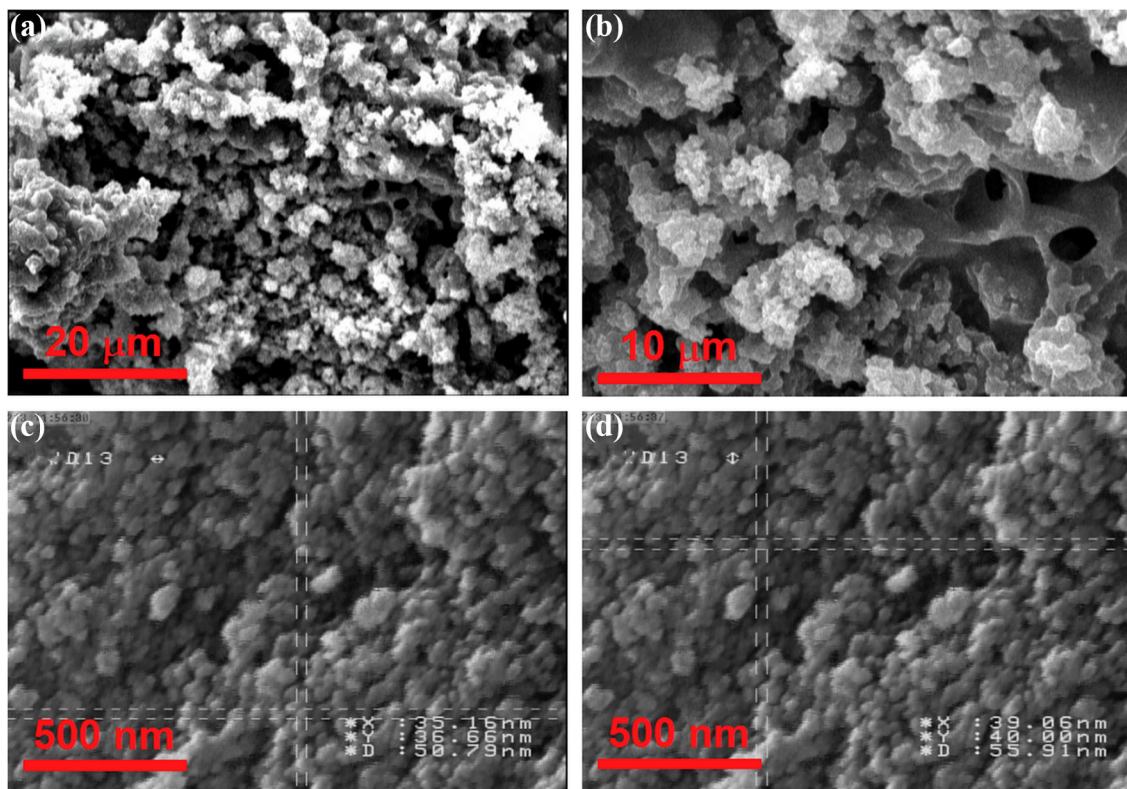


Fig. 3. SEM images of (a and b) PT-F and (c and d) Fe<sub>3</sub>O<sub>4</sub> nanoparticles.

broad and strong peak at 575 cm<sup>-1</sup> corresponds to Fe<sub>3</sub>O<sub>4</sub> and indicates successful synthesis of Fe<sub>3</sub>O<sub>4</sub> nanoparticles.<sup>52-54</sup>

Additionally, peaks in the region between 600 cm<sup>-1</sup> and 1500 cm<sup>-1</sup> are known as the fingerprints of polythiophene.<sup>53-55</sup> Appearance of a peak with wavenumber 582 cm<sup>-1</sup> in the PT-F spectrum, which is shifted about 7 cm<sup>-1</sup> to the right, indicates that polythiophene has been successfully doped with Fe<sub>3</sub>O<sub>4</sub>. Furthermore, in the PT-F spectrum, the peak at 934 cm<sup>-1</sup> is related to the stretching vibration of in-plane C-H.<sup>53</sup>

Figure 3 shows the SEM images of PT-F (a and b) and Fe<sub>3</sub>O<sub>4</sub> (c and d) nanoparticles. As this figure shows (c and d), the average size of Fe<sub>3</sub>O<sub>4</sub> nanoparticles is between 50 nm and 56 nm, while the PSA analysis (Fig. 4) points out that the average size of PT-F is 10 nm, which is five times smaller than Fe<sub>3</sub>O<sub>4</sub> nanoparticles. These results reveal that the doping process of polythiophene with Fe<sub>3</sub>O<sub>4</sub> not only can lead to a significant decrease in the average size of the synthesized nanoparticles, but also can improve the distribution and interaction of fillers within the matrix.

Figure 5a schematically shows the composition of bitumen along with PT-F nanoparticles, while parts (b) and (c) demonstrate the morphology of samples containing the neat bitumen and reinforced bitumen with 10 wt.% PT-F. Furthermore, Fig. 5b and c clearly shows that addition of PT-F to the 70 penetration-grade bitumen via the vacuum shock

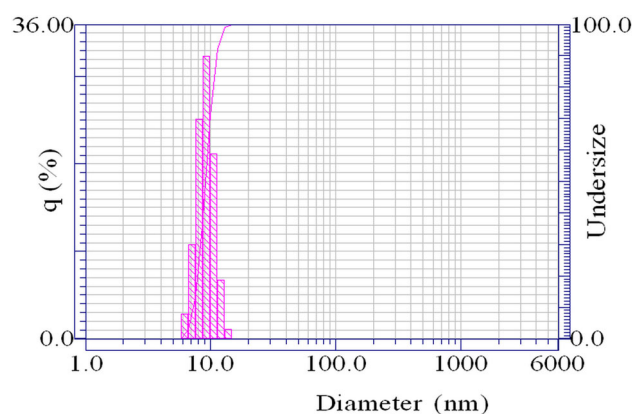


Fig. 4. PSA analysis results for PT-F nanoparticles.

technique has led to considerable improvement in the morphology of the developed samples in terms of reducing the overall number of voids and defects, which is due to good interaction and compatibility with the molten phase of bitumen.

### Rheological Properties of the Developed Samples

Figure 6a, b, c, and d shows the complex shear modulus of the neat and reinforced bitumen at diverse filler loadings versus frequency, temperature, time, and stress. As Fig. 6a shows, at higher frequencies (20–30 Hz), samples containing PT-F

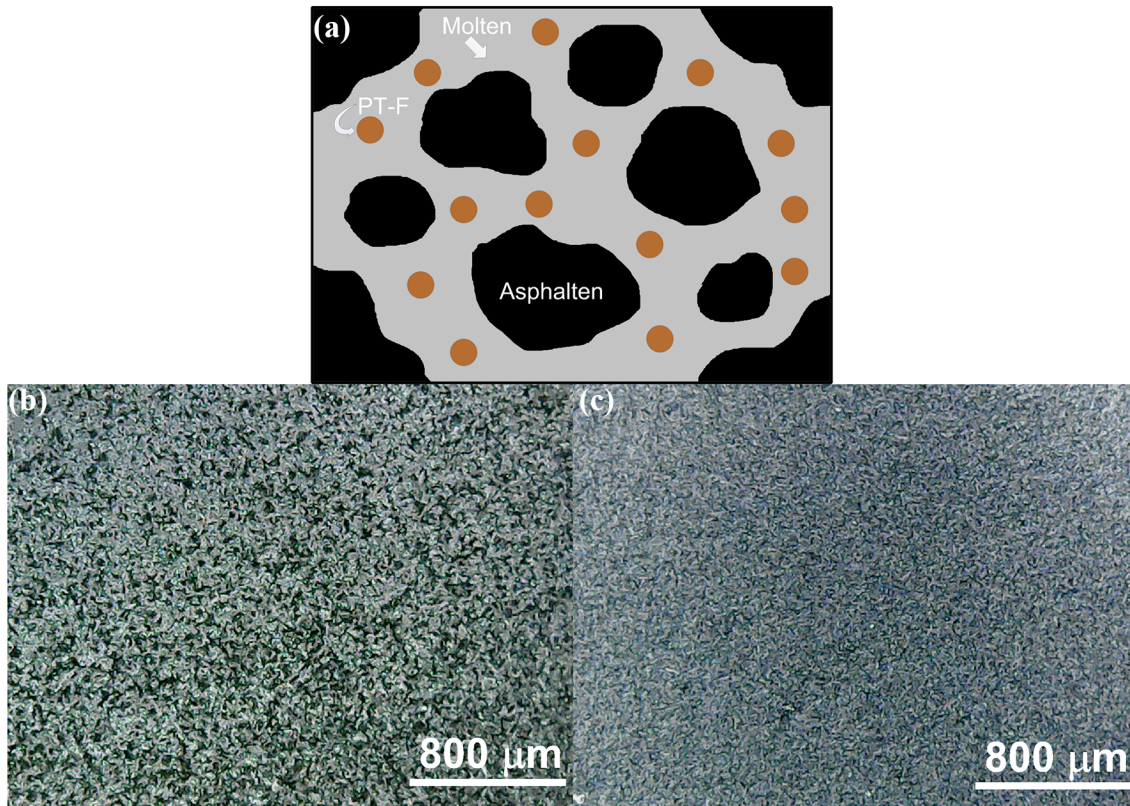


Fig. 5. (a) Schematic composition of the reinforced bitumen with PT-F,  $\times 1000$  digital optical imaging; (b) the neat bitumen; (c) the modified bitumen with 10 wt.% PT-F.

present much a higher complex shear modulus compared with the neat bitumen. In this case, at frequency loadings of 5 Hz, 20 Hz, and 30 Hz, the sample containing 10 wt.% PT-F showed 16.66%, 40.00%, and 29.31% improvement in the complex shear modulus compared with the neat bitumen, respectively, noting that the complex shear modulus is an indicator of stiffness or resistance against deformation.<sup>8</sup>

Moreover, in Fig. 6b, the effect of the low temperature test on the complex shear modulus is given. As this figure shows, the higher the applied temperature is, the higher the complex shear modulus. Accordingly, the reinforced sample containing 10 wt.% PT-F showed 66.66%, 38.29%, and 38.46% improvement at 5°C, 20°C, and 30°C compared with the neat bitumen, respectively.

Furthermore, Fig. 6c shows the effect of applied force time on the complex shear modulus. As this figure demonstrates, until 30 min, the reinforced samples presented a higher complex shear modulus, and after 50 min, the complex shear modulus leveled off, while the neat bitumen did not exhibit considerable changes.

As shown in Fig. 6d, under a varying stress load, the sample containing 10 wt.% PT-F expressed 52.94%, 57.81%, and 61.66% improvement in the complex shear modulus at 4 MPa, 8 MPa, and 12 MPa, respectively, compared with the neat

bitumen. Furthermore, both the reinforced and neat bitumen samples presented a constant complex shear modulus. In other words, modification of bitumen with PT-F can lead to significant improvement in the stiffness of bitumen and thus its resistance against deformation under applied forces.

In Fig. 7a, b, and c, the effect of PT-F at different filler loadings on the softening point, penetration, and reversibility can be seen, respectively. As shown in Fig. 7a, with an increase in the weight percentage of PT-F within the bitumen, the softening point rapidly increases. In this case, for specimens containing 10 wt.% PT-F, the softening point reaches approximately 90°C, which shows an approximately 40°C increase compared with the neat bitumen. Besides, in Fig. 7b, the effect of PT-F loading on the penetration of bitumen is evaluated. As can be seen, an increase in the filler loading led to a considerable decline in the penetration of the final composition. Besides, an increase in the filler loading can greatly enhance the reversibility rate of the final composition (Fig. 7c). In this case, with an increase in the weight percentage of PT-F to 10 wt.%, the reversibility rises to about 99%, which is a remarkable achievement. On the other hand, a significant increase in the softening point of the sample containing 10 wt.% PT-F (Fig. 7a) along with its appropriate complex shear modulus at low



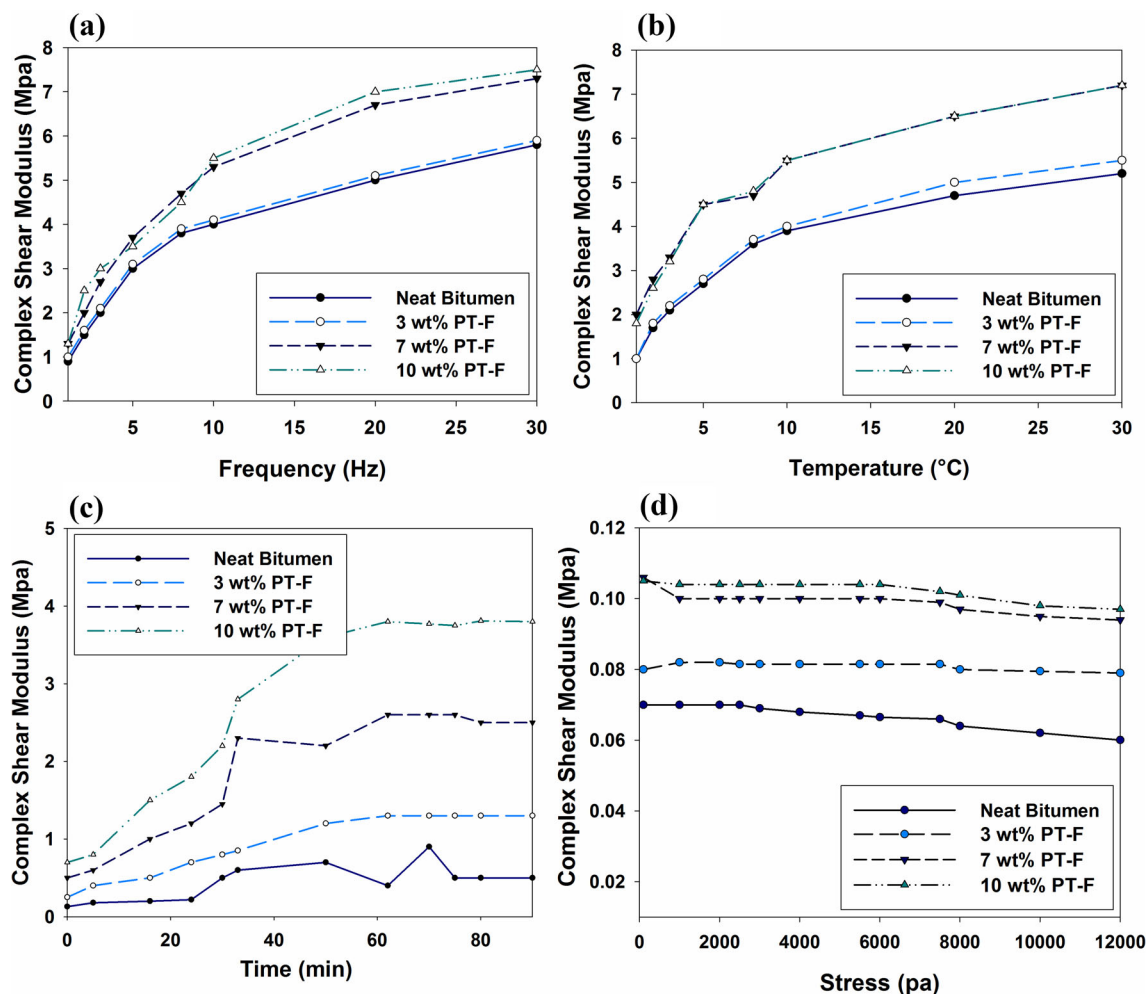


Fig. 6. Effect of PT-F at different filler loadings on the variation of complex shear modulus versus (a) applied frequency, (b) applied temperature, (c) test time, and (d) stress.

temperature range (0–30°C) is an indication of the remarkable increase in the resistance of reinforced samples against deformation and applied heat.

In Fig. 8a, and b, the effect of various filler loadings on the phase angle versus frequency and temperature can be seen. As shown in Fig. 8a, by an increase in the loading frequency, the phase angle for samples containing the modified and neat bitumen decreases. In this regard, both groups of samples presented viscoelastic behavior, while the modified samples showed a higher phase angle compared with the neat bitumen. In fact, by an increase in the weight percentage of PT-F, the samples showed more viscous behavior at low frequency loadings, while they were more elastic at high frequency loadings. On the other hand, as shown in Fig. 8b, by an increase in the applied temperature, the overall value of the phase angle increased, and the characteristics of both modified and unmodified samples changed from elastic

toward viscous though the modified samples are advantageously less viscous in the entire range.

In Fig. 8c, the dissipated energy of samples versus the number of cycles until failure is given. Moreover, Fig. 8c shows the resistance of samples against fatigue damage. As shown in this figure, an increase in the weight percentage of PT-F leads to significant improvement against cyclic loads, thereby avoiding fatigue crack growth and improving the average lifespan until failure, noting that failure due to the cyclic load is defined as the transition process between crack initiation and crack propagation.

The microstructure of each bituminous material during the tests is expressed by a steady change in the stress–strain relationships including the complex shear modulus, phase angle, and dissipated energy. However, a rapid change in the mechanical properties of bituminous materials can be attributed to unstable and coalescence crack propagation by means of molecular scission or rupture due to

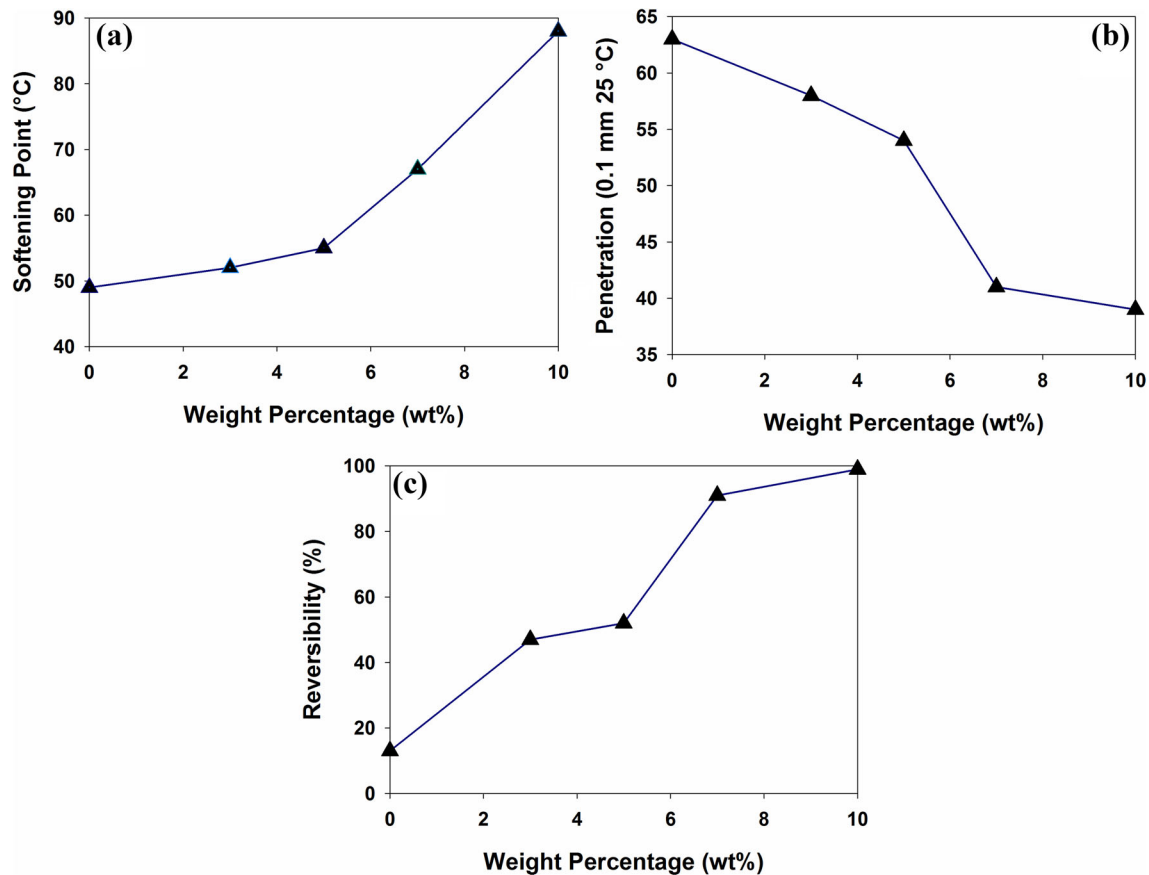


Fig. 7. Effect of PT-F at different filler loadings on (a) the softening point, (b) penetration, and (c) reversibility.

fatigue damage or cyclic load.<sup>44</sup> In this regard, the obtained results (Figs. 6d and 8c) indicate that the reinforced samples represent approximately invariant mechanical behavior over a wide range of applied forces (0–12 MPa). It is apparent that application of a cyclic load confirms the better performance of reinforced samples against fatigue damage and crack propagation.

## CONCLUSION

In this research, polythiophene—as the main filler—was doped with  $\text{Fe}_3\text{O}_4$  to enhance the bitumen characteristics as a construction and building material. The mixing process was facilitated by the vacuum shock technique. This work aimed to improve the resistance of bitumen whether against physical damage or UV–Vis degradation.

The FTIR examination confirmed the successful synthesis of PT-F, while the SEM and PSA analyses revealed that the average size of PT-F nanoparticles

was about 10 nm. This important decrease in the average size of particles yields a better interaction of PT-F with the molten phase of bitumen. Moreover, the results from the optical images showed that modification of bitumen with PT-F can significantly modify the morphology of the developed specimens.

In addition, evaluation of sample specifications via DSR and empirical rheological tests showed that modification of bitumen with PT-F at different filler loadings can highly improve their resistance against deformation, which can be gauged by considering the complex shear modulus and reversibility. All the samples presented an approximately constant complex shear modulus over a wide range of applied forces. The best performance was the maximum filler loading ratio under test (10 wt.% PT-F) regarding all measures under investigation. Therefore, in this working range, only the economy of production can be a limiting factor on the filler usage.



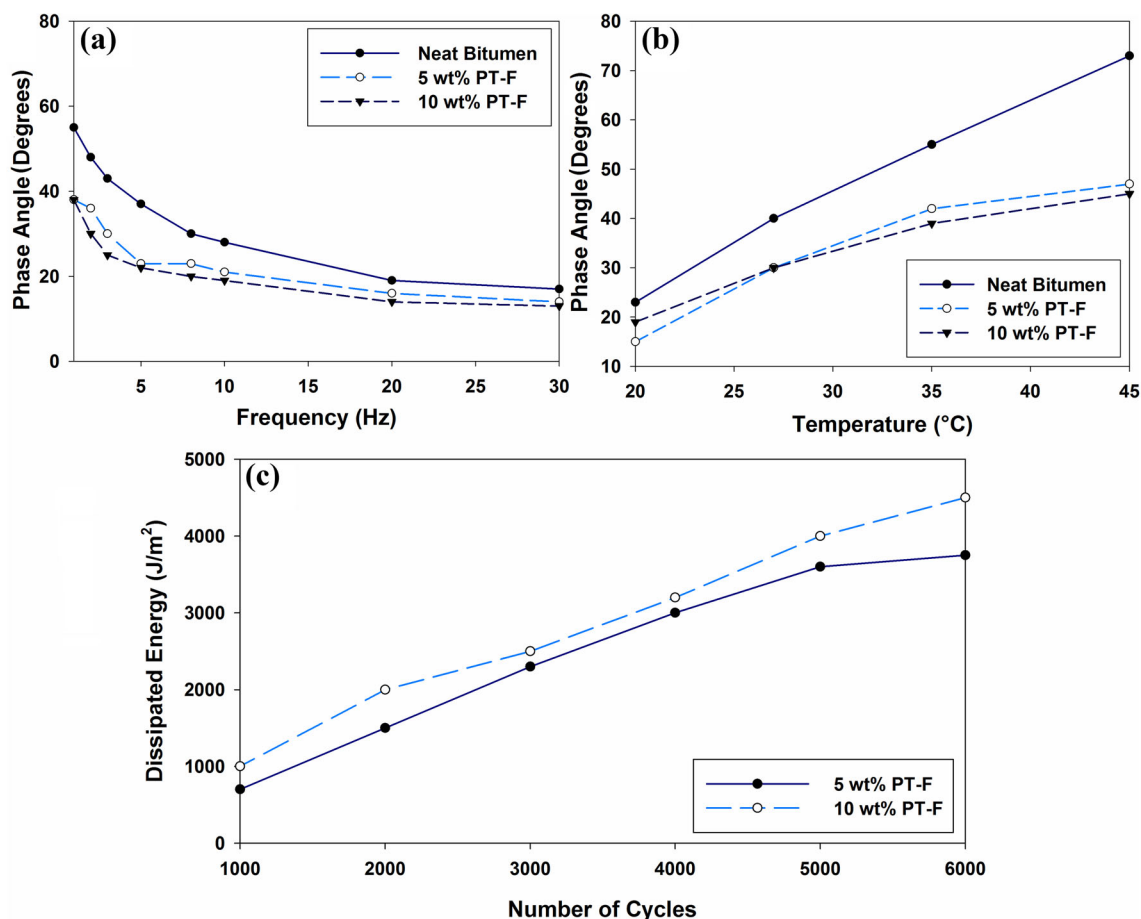


Fig. 8. Effects of PT-F at different filler loadings on (a) the phase angle versus loading frequency, (b) phase angle versus applied temperature, and (c) dissipated energy versus cycles until sample failure.

### CONFLICT OF INTEREST

The authors declare that they have no conflict of interest.

### ELECTRONIC SUPPLEMENTARY MATERIAL

The online version of this article (<https://doi.org/10.1007/s11837-018-3215-3>) contains supplementary material, which is available to authorized users.

### REFERENCES

- S.G. Jahromi and A. Khodaii, *Constr. Build. Mater.* 23, 2894 (2009).
- J. Read and D. Whiteoak, *The Shell Bitumen Handbook*, 5th ed. (London: Thomas Telford, 2003), p. 231.
- T.J. Pinnavaia and G.W. Beall, *Polymer-Clay Nanocomposites* (Chichester: John Wiley, 2000), p. 21.
- A. Kebritchi, A. Jalali-Arani, and A.A. Roghanizad, *Constr. Build. Mater.* 25, 2875 (2011).
- M.R. Karim, C.J. Lee, and M.S. Lee, *J. Polym. Sci., Part A: Polym. Chem.* 44, 5283 (2006).
- J.L. Goodrich, J.E. Goodrich, and W.J. Kari, *Asphalt Composition Tests: Their Application and Relation to Field Performance*, Transportation Research Record 1096 (Washington, DC: TRB, National Research Council, 1986) pp. 146–167.
- E.J. Van Assen and M. Van de Ven, *Review of South African Bitumen Specification to Take Cognisance of Compositional Balance Relative to Long-Term Behaviour* (Chennai: Department of Transport, 1996).
- S. Dessouky, C. Reyes, M. Ilias, D. Contreras, and A. Papagiannakis, *Constr. Build. Mater.* 25, 2785 (2011).
- M. Garcia-Morales, P. Partal, F. Navarro, and C. Gallegos, *Fuel* 85, 936 (2006).
- J.G. Speight, *The Chemistry and Technology of Petroleum*, 5th ed. (Boca Raton: CRC Press, 2014), pp. 187–240.
- S.S. Galooyak, B. Dabir, A.E. Nazarbeygi, and A. Moeini, *Constr. Build. Mater.* 24, 300 (2010).
- N. Baldino, D. Gabriele, F.R. Lupi, C.O. Rossi, P. Caputo, and T. Falvo, *Constr. Build. Mater.* 40, 397 (2013).
- G. Martinez-Arguelles, F. Giustozzi, M. Crispino, and G.W. Flintsch, *Constr. Build. Mater.* 72, 423 (2014).
- C. Wang, P. Wang, Y. Li, and Y. Zhao, *Constr. Build. Mater.* 80, 195 (2015).
- E. Garilli, F. Autelitano, C. Godenzoni, A. Graziani, and F. Giuliani, *Constr. Build. Mater.* 125, 352 (2016).
- L.G.A. Farias, J.L. Leitinho, B.D.C. Amoni, J.B. Bastos, J.B. Soares, S.D.A. Soares, and H.B. de Sant'Ana, *Constr. Build. Mater.* 125, 873 (2016).

17. D. Zhang, H. Zhang, C. Zhu, and C. Shi, *Constr. Build. Mater.* 144, 423 (2017).
18. C. Zhu, H. Zhang, C. Shi, and S. Li, *Constr. Build. Mater.* 146, 30 (2017).
19. A.K. Das and M. Panda, *Constr. Build. Mater.* 149, 724 (2017).
20. O. Xu, P.R. Rangaraju, S. Wang, and F. Xiao, *Constr. Build. Mater.* 154, 841 (2017).
21. S.M. Mousavi, M. Farsi, and M. Azizi, *J. Appl. Polym. Sci.* 132, 1 (2015).
22. S. Wu, J. Han, L. Pang, M. Yu, and T. Wang, *Constr. Build. Mater.* 33, 133 (2012).
23. Z. Feng, J. Yu, and S. Wu, *Constr. Build. Mater.* 29, 591 (2012).
24. H. Wu, L. Li, J. Yu, S. Xu, and D. Xie, *Constr. Build. Mater.* 111, 565 (2016).
25. J. Li, J. Yu, S. Wu, L. Pang, S. Amirkhanian, and M. Zhao, *Constr. Build. Mater.* 152, 832 (2017).
26. M.N. Siddiqui, M. Mansha, U. Mehmood, N. Ullah, A.F. Al-Betar, and A.A. Al-Saadi, *Dyes Pigm.* 141, 406 (2017).
27. I. Osaka, G. Sauve, R. Zhang, T. Kowalewski, and R.D. McCullough, *Adv. Mater.* 19, 4160 (2007).
28. M.L. Braunger, A. Barros, M. Ferreira, and C.A. Olivati, *Electrochim. Acta* 165, 1 (2015).
29. P. Sivaraman, S.P. Mishra, A.R. Bhattacharyya, A. Thakur, K. Shashidhara, and A.B. Samui, *Electrochim. Acta* 69, 134 (2012).
30. C. Zhang, H. Zhang, B. Du, R. Hou, and S. Guo, *J. Colloid Interface Sci.* 368, 97 (2012).
31. A. Gök, M. Omastová, and A.G. Yavuz, *Synth. Met.* 157, 23 (2007).
32. R. Elsenbaumer, K. Jen, G. Miller, and L. Shacklette, *Synth. Met.* 18, 277 (1987).
33. M.R. Chandra, P.S.P. Reddy, T.S. Rao, S. Pammi, K.S. Kumar, K.V. Babu, C.K. Kumar, and K. Hemalatha, *J. Phys. Chem. Solids* 105, 99 (2017).
34. D.E. Motaung, G.F. Malgas, C.J. Arendse, S.E. Mavundla, C.J. Oliphant, and D. Knoesen, *Sol. Energy Mater. Sol. Cells* 93, 1674 (2009).
35. R.D. McCullough, *Adv. Mater.* 10, 93 (1998).
36. J.J. Tindale, H. Holm, M.S. Workentin, and O.A. Semenkhin, *J. Electroanal. Chem.* 612, 219 (2008).
37. A. Abd-El-Aziz, S. Dalgakiran, I. Kucukkaya, and B. Wagner, *Electrochim. Acta* 89, 445 (2013).
38. F.M. Winnik, *Chem. Rev.* 93, 587 (1993).
39. E. González-Juárez, M. Güizado-Rodríguez, V. Barba, M. Melgoza-Ramírez, M. Rodríguez, G. Ramos-Ortiz, and J. Maldonado, *J. Mol. Struct.* 1103, 25 (2016).
40. S.A. Hashemi and S.M. Mousavi, *Compos. A* 90, 457 (2016).
41. S.A. Hashemi, S.M. Mousavi, M. Arjmand, N. Yan, and U. Sundararaj, *Polym. Compos.* 39, E1139 (2018).
42. S.A. Hashemi, S.M. Mousavi, R. Faghihi, M. Arjmand, S. Sina, and A.M. Amani, *Radiat. Phys. Chem.* 146, 77 (2018).
43. S.M. Mousavi, S.A. Hashemi, M. Arjmand, A.M. Amani, F. Sharif, and S. Jahandideh, *ChemistrySelect* 3, 7200 (2018).
44. A. Subhy, *Constr. Build. Mater.* 156, 28 (2017).
45. X. Lu and U. Isacsson, *Constr. Build. Mater.* 11, 23 (1997).
46. D.A. Anderson, D.W. Christensen, H.U. Bahia, R. Dongre, M. Sharma, C.E. Antle, and J. Button, *Strategic Highway Research Program, National Research Council*. Report No. SHRP-A-369 (1994).
47. G. Airey, *Rheological characteristics of polymer modified and aged bitumens*. Dissertation, University of Nottingham (1997).
48. S. Shen, G.D. Airey, S.H. Carpenter, and H. Huang, *Road Mater. Pavement Des.* 7, 47 (2006).
49. W. Van Dijk and W. Visser, Energy approach to fatigue for pavement design, in *Proceedings of the Association of Asphalt Paving Technologists Proceedings* (1977), pp. 1–40.
50. K. Ghuzlan and S. Carpenter, *Transp. Res. Rec.* 1, 141 (2000).
51. M.W. Barsoum, T. Zhen, S.R. Kalidindi, M. Radovic, and A. Murugaiah, *Nat. Mater.* 2, 107 (2003).
52. Y. Wei, B. Han, X. Hu, Y. Lin, X. Wang, and X. Deng, *Procedia Eng.* 27, 632 (2012).
53. F. Entezari Juybari, A. Kamran-Pirzaman, and M. Ghorbani, *Inorg. Nano Met. Chem.* 47, 121 (2017).
54. S.N.A. Baharin, N. Muhamad Sarih, and S. Mohamad, *Polymers* 8, 117 (2016).
55. R. Liu and Z. Liu, *Chin. Sci. Bull.* 54, 2028 (2009).